Effect of long-term natural aging on the microstructural characteristics of an extruded WE54 alloy

Hiba Azzeddine, Thierry Baudin, François Brisset

Effect of long-term natural aging on the microstructural characteristics of an extruded WE54 alloy

Hiba Azzeddine[1,*], Thierry Baudin[2] and François Brisset[2]

[1] Laboratory of Materials and Renewable Energy, Faculty of Sciences, Mohamed Boudiaf University, 28000, M'sila, Algeria.

[2] Université Paris-Saclay, CNRS, Institut de chimie moléculaire et des matériaux d'Orsay, 91405, Orsay, France.

* Corresponding author: Pr. Hiba Azzeddine, hiba.azzeddine@univ-msila.dz

Abstract

The microstructure and the corresponding crystallographic texture of the as-extruded WE54 alloy after natural aging for 11 years at room temperature have been characterized by the Electron backscatter diffraction (EBSD) technique. Before natural aging, the as-extruded WE54 exhibited equiaxed microstructure with a strong splitting basal texture and the presence of $Mg_{24}Y_5$ and $Mg_{41}Nd_5$ second particles along the extrusion direction (ED). Unexpectedly, long-term aging led to the formation of elongated deformed grains along ED having {11-20}<11-10> and {0001}<10-10> orientations with a partial development of fine static recrystallized grains by continuous and discontinuous mechanisms. It is believed that the origin of such grain structure development is the residual stored strain during the extrusion processing and the strain field induced from the solute Nd and Y atoms diffusion through the long-term natural aging. Artificial aging at 400 °C for 60 min demonstrated that the elongated deformed grains disappeared and left behind a heterogeneous recrystallized microstructure with a weak basal texture.

Keywords: Deformation; Natural aging; Magnesium; Rare-earth.

1. Introduction

In the past decade, magnesium-containing rare-earth elements (Mg-RE) alloys have gained great attention in research and industrial applications for the beneficial effect of RE elements on improving the mechanical properties of Mg-based alloys like low-temperature strength and high-temperature creep resistance [1-4]. The improvement of mechanical properties is a direct consequence of activation enhancement of non-basal dislocation slip systems, grain refinement, and texture weakening of Mg-RE alloys [5-7]. The main responsible mechanisms for the microstructural and textural modifications observed in Mg-RE alloys are principally related to the RE solute drag and Zener pinning of second phases which are effective obstacles for the grain boundary mobility and dislocation glide [2, 4]. Accordingly, the influence of thermomechanical processing and artificial aging on the microstructure especially the precipitation behaviour and mechanical properties are widely investigated in Mg-RE alloys to control their design with better properties [8-15]. Nevertheless, only a few investigations can be found in the literature dealing with the impact of natural aging on the hardening behaviour of Mg-RE alloys [16-21]. Age-hardening was noticed in binary Mg-15Gd and Mg-13Tb (wt.%) alloys during natural aging at room temperature for 1 month due to the clustering of solute atoms and vacancies [16]. Natural aging for 3 years leads to a reduction in the deformation structure and precipitation of the second phase in the as-extruded Mg-10Gd-2Y-0.8Zr (wt.%) alloy [17]. However, the evolution of grain structure and texture through natural aging is lacking since the investigations mentioned above were conducted at the atomic scale by using positron lifetime spectroscopy, high-angle annular dark field, or scanning transmission electron microscopy techniques [16-20]. For the first time, the present work presents the evolution of microstructure and texture of as-extruded WE54 (Mg-Y-Nd-Zr) alloy after long-term natural aging of 11 years using electron backscatter diffraction (EBSD) technique. In the past, the WE54 (Mg-4.9Y-4.2Nd-0.56Zr, wt.%) alloy was the subject of different investigations dealing with the effect of deformation processing and annealing treatments on the evolution of microstructure, texture, precipitation and mechanical properties [8-12].

2. Experimental procedure

The initial WE54 alloy with dimensions of 100 (ED) × 60 (TD) × 14 (ND) mm^3 was generously provided by Chinese collaborators in an as-extruded condition [8]. Here, ED, TD and ND mean extrusion direction, transverse direction and normal direction, respectively. Accordingly, the alloy was prepared in an electric resistance furnace and followed by a hot extrusion at 400 °C

with an extrusion ratio of 8:1 [8]. Rectangular samples with dimension of 14 (ED) ×10 (TD) ×6 (ND) mm^3 were machined from the block and exposed to normal indoor atmosphere in M'sila, Algeria, for 11 years. During each year, the temperature in M'sila city varies usually from 40 °C (in summer) to 1 °C (in winter).

Optical microscopy observations were performed on ED-TD plane of the natural-aged sample after mechanical grinding and electropolishing with 5:3 of ethanol and phosphoric acid for 30 min and then etching for 3 s in a 5% HNO_3, 15% CH_3CO_2H, 60% C_2H_5OH, and 20% H_2O.

The distribution and the composition of second phases particles were characterized by scanning electron microscopy (SEM, FEG-SEM ZEISS Gemini) equipped with energy dispersive spectrometry (EDS) system in backscattering (BSE) mode operated at 15 kV. At least three SEM photos were used to calculate their mean size and volume fraction by ImageJ software.

An EBSD area of 800 × 800 μm^2 with a step size of 0.5 µm was measured from the natural-aged sample (in the ED-TD plane) using a FEG-SEM SUPRA 55 VP field emission gun scanning electron microscope operating at 20 kV. The EBSD data were examined using the TSL Orientation Imaging Microscopy (OIM™) software. The kernel average misorientation (KAM) method was applied to determine the distribution of local distortions in the grains [22]. For that, the local misorientation was calculated from the mean misorientation angle between the point and its 3^{th} neighbor and excluding misorientations greater than 15°. In addition, the grain orientation spread (GOS) approach was used to separate the recrystallized grains from the deformed ones [23]. GOS is known as the average deviation between the orientation of each point in the grain and the average orientation of the grain [23]. Usually, the recrystallized grains (strain free grains) are identified as grains with GOS < 1° [23].

MTEX software was used to analyze the crystallographic texture by calculating the orientation distribution function (ODF) using the harmonic method (L = 22), and a gaussian function with a half-width of 5° [24].

3. Results and discussion

Figure 1 shows the optical micrograph and SEM photo with EDS analysis of the as-extruded and natural-aged WE54 samples, respectively. It is important to note that the as-extruded sample exhibits a homogeneous microstructure formed of equiaxed grains with an average grain size of 10 µm and the presence of dispersed second particles in the form of large bands along ED. The volume fraction of second phase particles estimated from the SEM photos of the as-extruded sample (Figure 1b) was found around 9 % and their mean size was 1.5 µm. The EDS analysis in different points (1–3) shown in Figure 1b indicates that the second particles contain

the Nd and Y elements (points 2 and 3) and could belong to the metastable ($Mg_{12}NdY$) and/or equilibrium ($Mg_{14}Nd_2Y$) precipitate phases. The Mg matrix (point 1) contains 4.7% of Y element and 3.5% of Nd element which is similar to the composition of commercial WE54 alloy (Mg-4.7-5.5Y-2-4Nd-0.4Zr, wt.%). The presence of different second particles in the as-extruded sample indicates that the precipitation occurred during the extrusion condition and cooling.

The microstructure of the natural-aged sample shown in Figures 1d and 1e presents some differences from the as-extruded WE54 sample. Concerning the particles, they form a typical streamline shape along ED but their fraction is slightly lower at ~ 7.5% and their mean size increases to 4.5 µm. The EDS analysis shown in Figure 2e indicates that the Mg matrix (point 4) contains only 2.6% of Y and no Nd element. In addition, the second particle (point 5) shows different Y and Nd concentrations than point 2 or point 3 indicating the dissolution of the precipitate phases. The change of Mg matrix and second phases is due to the diffusion of solute elements (Y and Nd) during the long-term natural aging (11-years).

It is apparent that the diffusion of Nd in Mg is faster than Y element. Indeed, it has been reported that heavy RE elements like Y and Gd have lower diffusivity in Mg than light RE elements such as Nd and Ce [25, 26]. The main apparent difference is the increase of grain size (~18 µm) and the development of new kind of bands along ED as shown in the blue frame in Figure 2d. The magnification of blue frame demonstrated that one of these bands contains inside fine grain (named zone 1) and the second kind of band (named zone 2) does not contain grains. Figures 1c and 1f show the texture of the as-extruded and natural-aged WE54 samples in term of {0002} recalculated pole figure, respectively. The as-extruded sample exhibited a strong basal texture (7.1 mrd, multiple random of distribution) with a split from ND towards TD. The split of the basal plane is caused by the activation of the <c + a> pyramidal slip system [5]. The as-extruded texture of the present WE54 alloy is slightly different from that reported for conventional Mg based alloys and this was attributed to the effect of RE elements [27-29]. The texture of natural-aged sample is obviously weaker (2.5 mrd) and shows the formation of a new texture component identified as the {11-20}<10-10>, (φ_1 = 30°, ϕ = 90°, φ_2 = 90°) component [30] as shown by the arrows in Figure 1f.

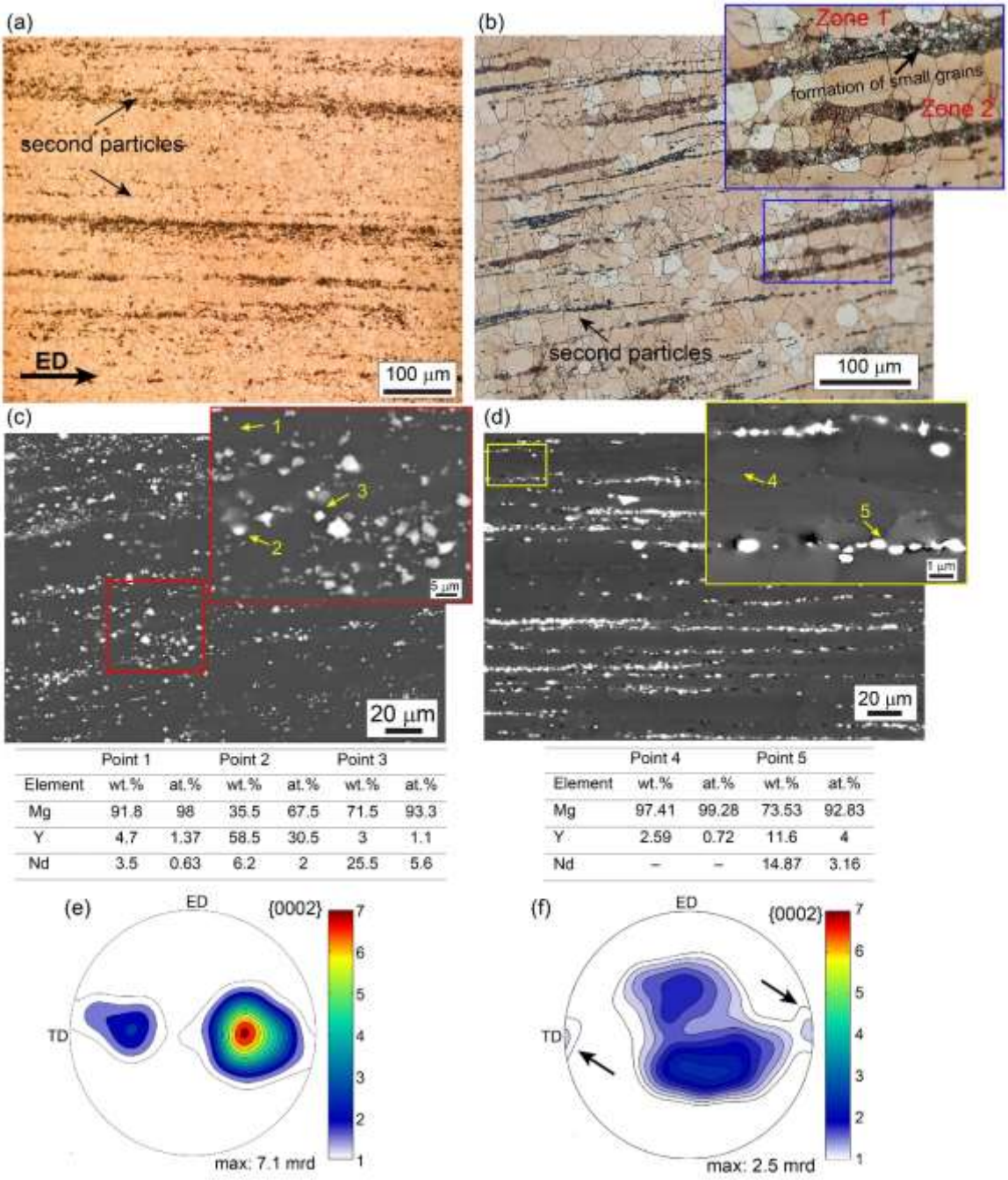

	Point 1		Point 2		Point 3	
Element	wt.%	at.%	wt.%	at.%	wt.%	at.%
Mg	91.8	98	35.5	67.5	71.5	93.3
Y	4.7	1.37	58.5	30.5	3	1.1
Nd	3.5	0.63	6.2	2	25.5	5.6

	Point 4		Point 5	
Element	wt.%	at.%	wt.%	at.%
Mg	97.41	99.28	73.53	92.83
Y	2.59	0.72	11.6	4
Nd	–	–	14.87	3.16

Figure 1: Optical micrograph, SEM photo with EDS analysis and {0002} recalculated pole figure of (a, b, c) as-extruded, and (d, e, f) natural-aged WE54 alloy, respectively.

Figures 2a shows a large inverse pole figure (ND-IPF) map coupled with Image Quality (IQ) of the natural-aged WE54 sample. The black zones parallel to the ED present the alignment of the second particles. As evidence, the microstructure of the natural-aged sample shows the presence of several elongated bands along the ED (~168 µm) with a single orientation mostly having red and green colours (see the white arrows). The red grains represent <0001> // ND oriented grains and the green grains should represent <11-20>//ND oriented grains. In order to

identify the orientation of theses elongated grains, the ED-IPF map is presented in Figure 2b. As can be observed, the green and red grains have their <10-10>//ED. Hence, the red grains exhibit the {0001}<10-10> component with a deviation of 20° from its ideal position, whereas the green grains display the {11-20}<10-10> texture component with a deviation of 15° as demonstrated in the IQ map shown in Figure 2c and the corresponding {0002} pole figures. Both components belong to the prismatic orientation (ED // <10-10>) which is often reported in as-extruded Mg-based alloys [15, 31-33]. The volume fraction of these elongated grains is around 5 %.

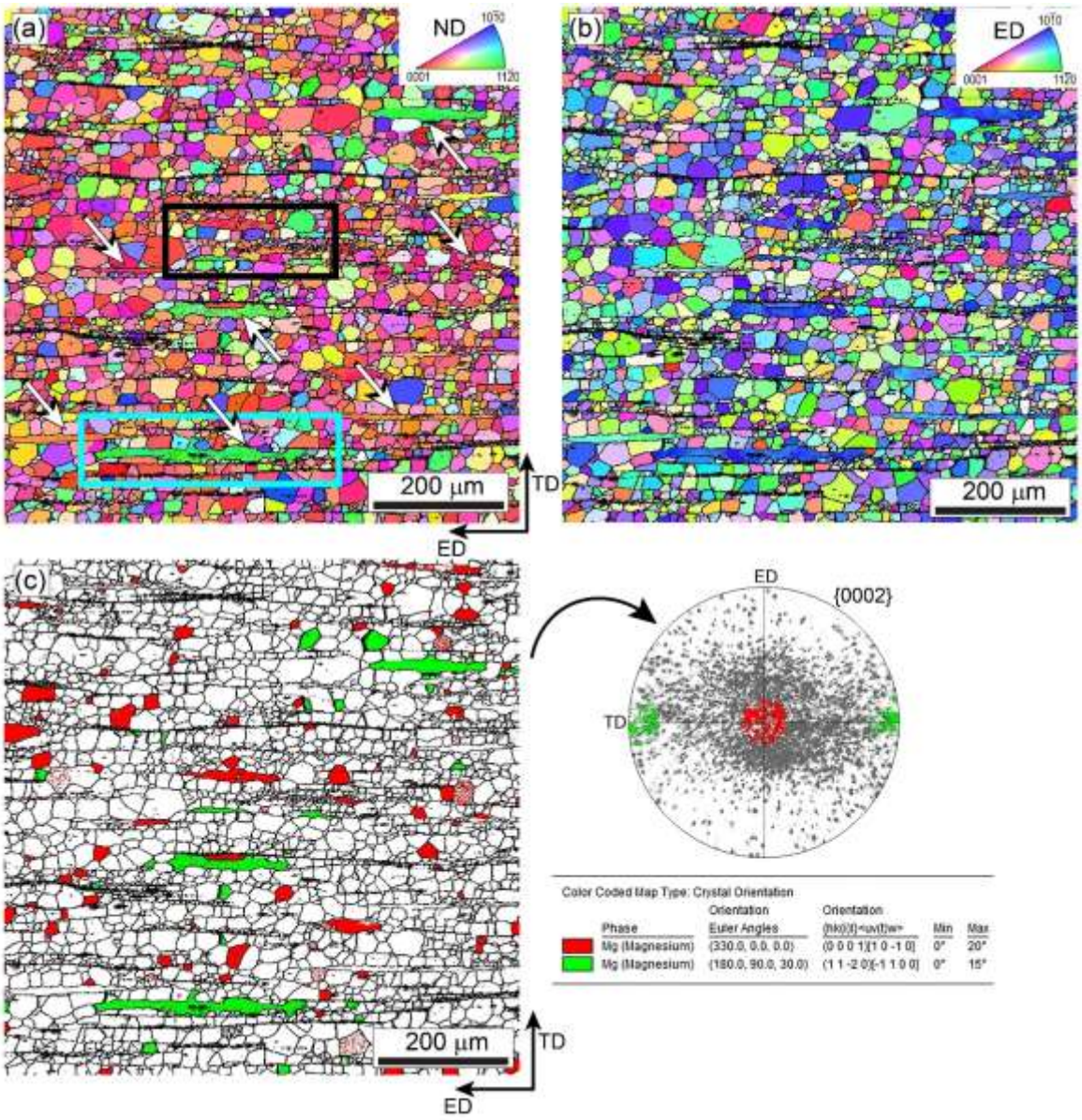

Figure 2: (a) ND-IPF, (b) ED-IPF maps coupled with IQ of natural-aged WE54 sample, (c) IQ map and the corresponding {0002} pole figure showing the red elongated grain with {0001}<10-10> texture component and the green elongated grains with {11-20}<10-10>.

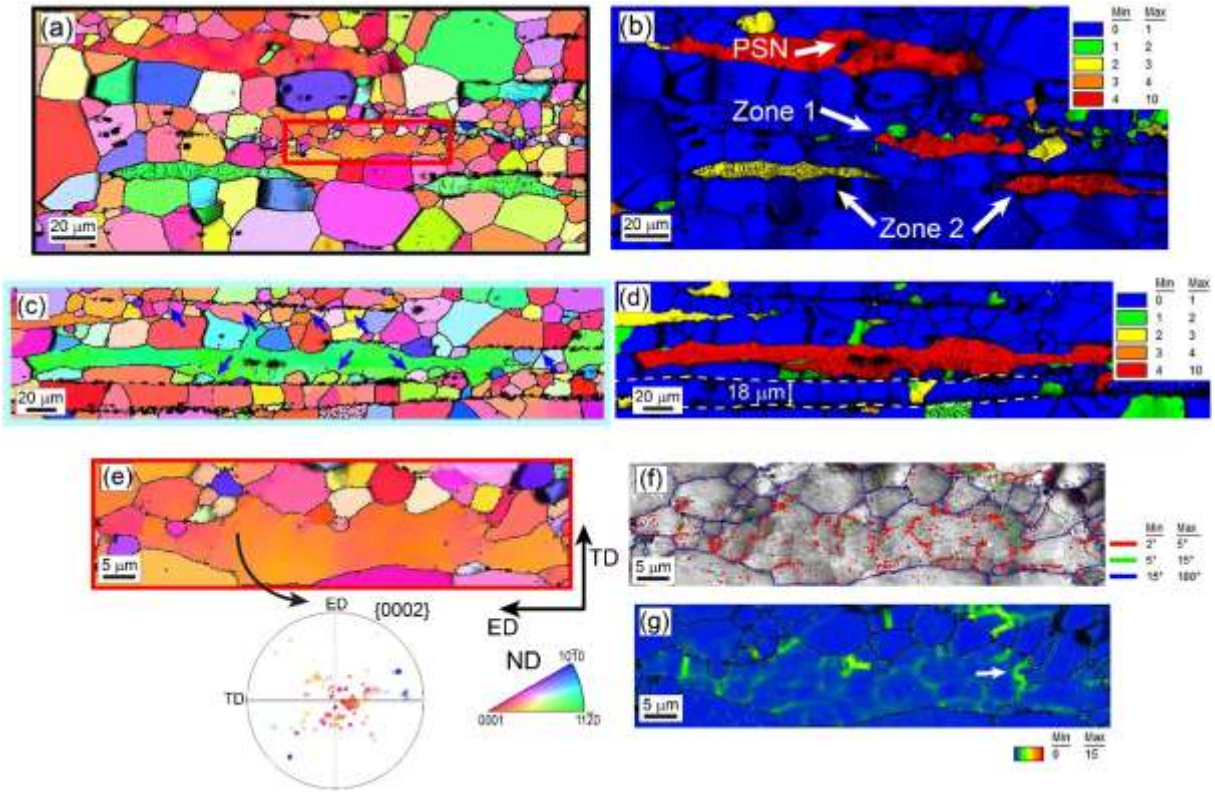

Figure 3: (a, b) and (c, d) ND-IPF and GOS maps of the magnification of the black and blue frames indicated in Figure 2a, respectively. (e, f, g) ND-IPF map with the corresponding {0002} pole figure, IQ map overlapped with grain boundary types and KAM map of the magnification of the red frame indicated in Figure 3a, respectively.

The zoom of black and blue frames (see Figure 2a) shown in Figures 3a and 3c presents interesting microstructural features characteristics. First, the elongated grains are deformed as evidenced from the GOS maps (Figures 3b and 3d). As can be seen from the magnification of red rectangle shown in Figure 3a and presented in Figure 3e, fine recrystallized grains (blue color in the GOS map) with mean grain size of about 4.2 µm are located at the grain boundaries of the red elongated grain which correspond to the zone 1 shown in Figure 1d. The green elongated grains in Figure 3a did not show any formation of grains which correspond to zone 2 already shown in the optical micrograph (Figure 1d). However, some fine recrystallized grains can be observed at the grain boundaries of the green elongated grain as shown in Figures 3c and d.

It is interesting to note that these fine grains have necklace-like structure similar to the resultant microstructure of discontinuous static recrystallization, i.e., serration, bulging and migration of high-angle boundaries of the deformed grain [34]. The fine grains formed along the grain boundaries of the red elongated grain have basal and also different orientations as is evident by

the corresponding {0002} pole figure (Figure 3e) which explains the texture weakening of the natural-aged sample.

Figures 3f and 3g show the IQ map overlapped with grain boundary types: high angle grain boundaries (HAGBs, $\theta > 15°$) in blue line colour, low angle grain boundaries (HAGBs, $5° < \theta < 15°$) in green line colour, and sub-grain boundaries ((HAGBs, $2° < \theta < 5°$) in red line colour and KAM map of the magnification of the red rectangle, respectively. As can be seen, the interior of the red elongated grain contains sub-grain boundaries which correspond to the occurrence of continuous static recrystallization [34]. The sub-grain boundaries are formed by the dislocation rearrangement as is evident from the high density of geometrically necessary dislocation (GNDs) in the KAM map (region with green colour). Some LAGBs can be observed mainly concentrated in the sub-grain boundaries resulting from the accumulation of dislocations. The KAM map shows that GNDs density is higher where the LAGBs exist. In fact, some sub-grains start to form near the grain boundary of the red elongated grain as indicated by the arrow in Figure 3g.

Moreover, it is obvious from Figures 3c and d that the second particles have great influence on the grain structure. First, Figures 3a and b are evidence for the occurrence of a particle stimulated nucleation (PSN) mechanism [35] inside the red elongated grain in which fine grains with completely different orientations than the basal component are formed around the second phase particles. Second, the dashed white lines shown in Figure 3d indicate the presence of relatively large grains having the size of the distance between the two second phase bands (around 18 µm). Meanwhile, the blue arrows indicated in Figure 3c show that the fine recrystallized grains cannot grow across the second particle band due to their Zener pinning effect on the grain boundaries which inhibited grain growth.

In order to further analyse the evolution of these elongated deformed grains, the natural-aged sample was subjected to artificial aging at 400 °C for 10 and 60 min and their microstructural and textural evolutions are presented in Figure 4, respectively.

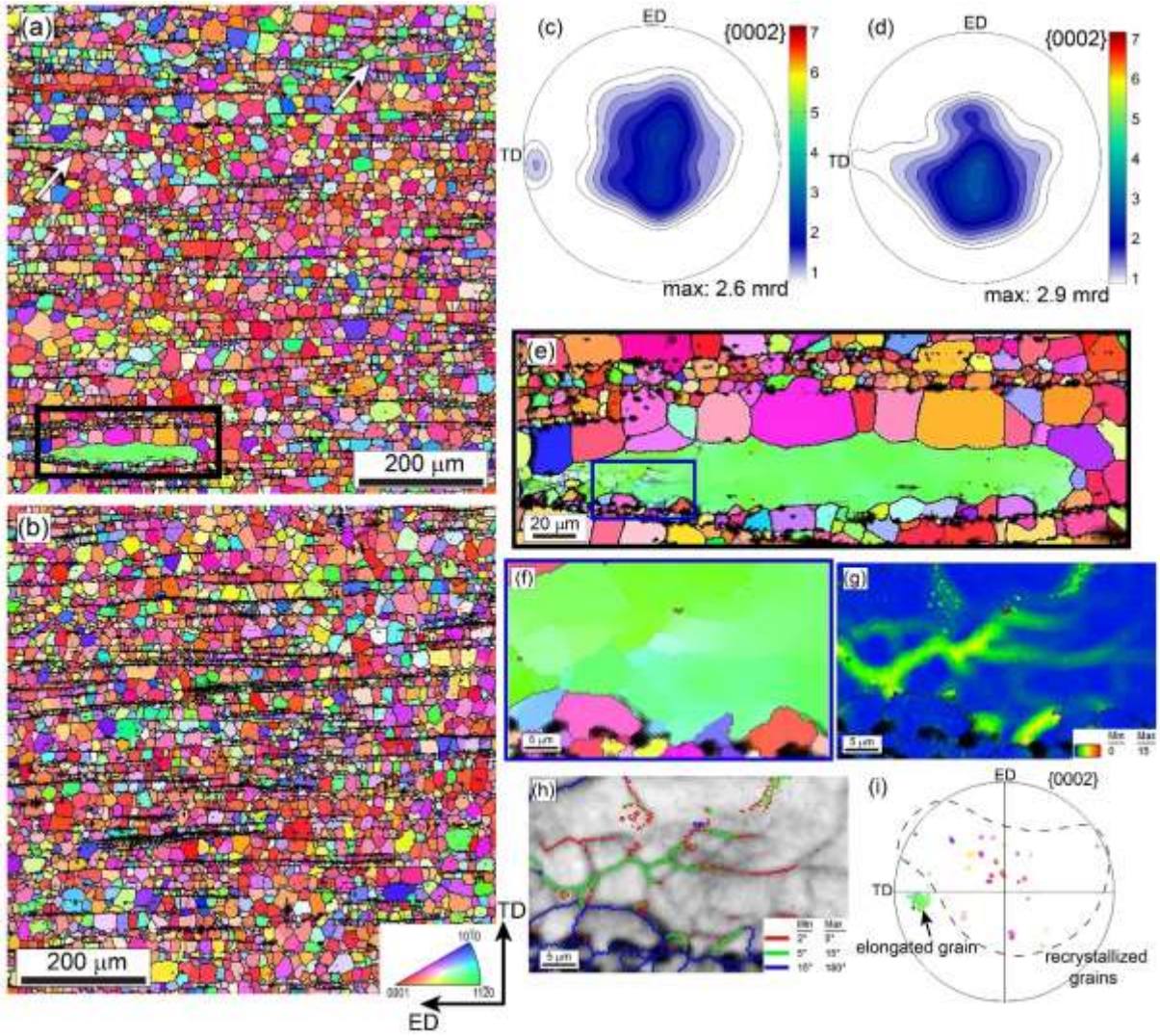

Figure 4: (a, c) and (b, d) ND-IPF map and {0002} recalculated pole figure of natural-aged WE54 sample after artificial aging at 400 °C for 10 min and 60 min, respectively. (e) ND-IPF map of the magnification of the black frame indicated in Figure 3a. (f, g, h, i) IPF, KAM and grain boundary type maps and corresponding {0002} pole figure of the zoom of the region in the blue rectangle indicated in Figure 3e.

The fraction of elongated grains decreases to 2.4 % after annealing for 10 min and disappeared after 60 min of annealing. Most of the remaining elongated grain have the {11-20}<10-10> orientation (green grains) as indicated by the white arrows in Figure 4a. Consequently, it can be concluded that the fine recrystallized grains are preferably formed along the red elongated grains (with {0001}<10-10> orientation). Nevertheless, the {11-20}<10-10> component disappeared with increasing annealing time as is evident from the {0002} recalculated pole figures shown in Figures 4c and 4d.

Figure 4e displays the microstructure around the green elongated grain after annealing for 10 min (black frame shown in Figure 4a). The microstructure remains obviously heterogeneous mostly formed of large and fine grains due to the effect of second phase particle bands. The distribution of fine grains in bands through the alignment of the particles is clearly visible. In addition to the occurrence of discontinuous static recrystallization in the green elongated grain, continuous static recrystallization is evident by the IPF, KAM and grain boundary type maps of the blue frame magnification (see Figure 4e) shown in Figures 4f-h. The corresponding {0002} pole figure of this region indicates that the new grains formed around the green elongated grain have a different orientation centred around the basal orientation. Also, the split of the basal pole disappears with annealing time leading to the formation of a weak typical basal texture. In the literature, it was observed that the weak texture developed in the early stage of static recrystallization is progressively replaced by a strong basal texture due to the preferential grain growth of the basal oriented grains (high mobility of 30° <0001> grain boundaries) [36]. However, the texture evolution after artificial aging remains weak due to the effect of RE elements (Nd and Y) on changing the grain boundary mobility through the solute drag and Zener pinning [2]. Finally, the microstructure of the sample annealed for 60 min exhibits a typical extrusion microstructure formed principally of large recrystallized grains and bands of fine recrystallized grains distributed along ED. This grain structure is very similar to the initial as-extruded WE54 sample (Figure 1a) with an exception of larger mean grain size of 19.5 µm. From the above observations, the artificial aging of the natural-aged WE54 alloy demonstrated that the elongated grains formed during natural aging are indeed deformed and gradually transformed to recrystallized grains by static recrystallization phenomena.

It should be noted that the development of coarse elongated grains along ED is frequently reported in Mg-based alloys after extrusion processing [15, 31-33]. These elongated grains are deformed and often have a ED//<10-10> prismatic orientation [15, 31-33] which is very similar to the microstructure obtained after natural aging. The development of such grain structure is attributed to the increasing strain which causes the alignment of material flow with respect to the deformation direction and the limited dynamic recrystallization during extrusion processing [15, 32]. It was reported that the origin of formation of prismatic orientation is the high activation of the prismatic slip system [37]. The volume fraction of the elongated un-recrystallized grains depends strongly on the extrusion conditions such as deformation temperature and extrusion ratio [15, 32].

It was expected that the natural aging will cause age-hardening/age-softening or even grain growth but it seemed implausible that the natural-aged WE54 alloy will develop a typical

extrusion deformation microstructure since no deformation was applied. Moreover, the extrusion sate of WE54 alloy exhibited already an equiaxed microstructure as demonstrated in Figure 1a. The exact origin of the development of elongated deformed grains during the natural ageing of the as-extruded WE54 alloy was not known in the present study. Nevertheless, it can be speculated that the amount of residual strain energy stored during extrusion processing in the form of microstructure defects, such as vacancies, dislocations and cell structures, is a plausible reason. In addition, the change in the Mg matrix and the second phases concentration shown in Figure 1e indicated that the diffusion of solute Nd and Y atoms through the 11 years can bring an additional strain field in the microstructure. It appears that the released strain field has a form of shape memory effect to form elongated grains along the ED similar to the elongated un-recrystallized grains developed during extrusion processing. However, further investigations are now required to explore the factors influencing the development of the deformation microstructure during the natural aging of the as-extruded WE54 alloy.

4. Conclusion

The effect of natural aging at room temperature on the microstructure and texture of the as-extruded WE54 alloy was characterized using EBSD and the main conclusions can be summarized as follows:

- The as-extruded microstructure is composed of equiaxed grains with a strong splitting basal texture and second particles bands along ED.
- Long-term natural aging for 11 years leads to the formation of elongated deformed grains along ED with partial development of fine static recrystallized grains by continuous and discontinuous manner.
- The concentration of Y and especially Nd elements is significantly reduced in the Mg-matrix. The composition of second phase is also modified but their distribution remains in bands along ED.
- The origin of the formation of elongated deformed grains along ED could be the residual strain energy stored during the extrusion processing and strain field induced by the diffusion of solute Nd and Y atoms through the natural aging.
- Artificial aging at 400 °C for 60 min demonstrated that the elongated deformed grains vanished and left behind a heterogeneous microstructure with a weak basal texture.

Acknowledgements: Prof. Rongshi Chen, and Dr. Enhou Han from the Institute of Metal Research, Chinese Academy of Sciences, China, are gratefully acknowledged for providing the WE54 alloy. The authors are grateful to Prof. T. G. Langdon from Materials Research Group, Department of Mechanical Engineering, University of Southampton, U.K., for his valuable help.

Data Availability: The raw/processed data required to reproduce these findings cannot be shared at this time as the data also forms part of an ongoing study.

References

[1] I.-H. Jung, M. Sanjari, J. Kim, S. Yue, Role of RE in the deformation and recrystallization of Mg alloy and a new alloy design concept for Mg–RE alloys, Scripta Materialia 102 (2015) 1-6.
[2] A. Imandoust, C.D. Barrett, T. Al-Samman, K.A. Inal, H. El Kadiri, A review on the effect of rare-earth elements on texture evolution during processing of magnesium alloys, Journal of Materials Science 52(1) (2017) 1-29.
[3] Y. Yang, X. Xiong, J. Chen, X. Peng, D. Chen, F. Pan, Research advances in magnesium and magnesium alloys worldwide in 2020, Journal of Magnesium and Alloys 9(3) (2021) 705-747.
[4] J. Xie, J. Zhang, Z. You, S. Liu, K. Guan, R. Wu, J. Wang, J. Feng, Towards developing Mg alloys with simultaneously improved strength and corrosion resistance via RE alloying, Journal of Magnesium and Alloys 9(1) (2021) 41-56.
[5] S.R. Agnew, M.H. Yoo, C.N. Tomé, Application of texture simulation to understanding mechanical behavior of Mg and solid solution alloys containing Li or Y, Acta Materialia 49(20) (2001) 4277-4289.
[6] Y. Chino, M. Kado, M. Mabuchi, Enhancement of tensile ductility and stretch formability of magnesium by addition of 0.2wt%(0.035at%)Ce, Materials Science and Engineering: A 494(1) (2008) 343-349.
[7] S. Sandlöbes, M. Friák, J. Neugebauer, D. Raabe, Basal and non-basal dislocation slip in Mg–Y, Materials Science and Engineering: A 576 (2013) 61-68.
[8] X. Liu, R. Chen, E. Han, High temperature deformations of Mg–Y–Nd alloys fabricated by different routes, Materials Science and Engineering: A 497(1) (2008) 326-332.
[9] H. Azzeddine, D. Bradai, Texture and Microstructure of WE54 Alloy after Hot Rolling and Annealing, Materials Science Forum 702-703 (2012) 453-456.
[10] H. Azzeddine, D. Bradai, On the texture and grain growth in hot-deformed and annealed WE54 alloy, International Journal of Materials Research 103(11) (2012) 1351-1360.
[11] H. Azzeddine, D. Bradai, On some aspects of compressive properties and serrated flow in Mg-Y-Nd-Zr alloy, Journal of Rare Earths 31(8) (2013) 804-810.
[12] S. Tighiouaret, H. Azzeddine, A. Sam, A. Sari, B. Alili, D. Bradai, On the Precipitation Behavior at 250 and 300 °C of WE54 Supersaturated Solid Solution, Advanced Materials Research 629 (2013) 85-89.
[13] S. Tighiouaret, R. Lachhab, A. Hanna, H. Azzeddine, Y. Huang, T. Baudin, A.-L. Helbert, F. Brisset, D. Bradai, T.G. Langdon, Thermal Stability of an Mg–Nd Alloy Processed by High-Pressure Torsion, Advanced Engineering Materials 21(12) (2019) 1900801.

[14] Y.I. Bourezg, H. Azzeddine, M. Harfouche, D. Thiaudiere, C. Mocuta, Y. Huang, D. Bradai, T.G. Langdon, An investigation by EXAFS of local atomic structure in an Mg-Nd alloy after processing by high-pressure torsion and ageing, Materials Letters 264 (2020) 127379.
[15] T. Zhao, Y. Hu, C. Zhang, B. He, T. Zheng, A. Tang, F. Pan, Influence of extrusion conditions on microstructure and mechanical properties of Mg-2Gd-0.3Zr magnesium alloy, Journal of Magnesium and Alloys 10(2) (2022) 387-399.
[16] J. Čížek, B. Smola, I. Stulíková, P. Hruška, M. Vlach, M. Vlček, O. Melikhova, I. Procházka, Natural aging of Mg–Gd and Mg–Tb alloys, physica status solidi A 209(11) (2012) 2135-2141.
[17] Z. Yang, H.B. Duan, Z.H. Wang, Y.C. Guo, P.H. Gao, J.P. Li, Effect of natural ageing on microstructure and mechanical properties of Mg–10Gd–2Y–0.8Zr Alloy, Materials Science and Engineering: A 648 (2015) 140-145.
[18] J. Zheng, Z. Li, B. Chen, Segregation of rare earth atoms in Mg-Gd-Y-Zr alloy after a 6-year natural ageing at room temperature: Atomic-scale direct imaging, Materials Letters 174 (2016) 86-90.
[19] M. Vlček, J. Čížek, O. Melikhova, P. Hruška, I. Procházka, M. Vlach, I. Stulíková, B. Smola, Early stages of precipitation in Mg-RE alloys studied by positron annihilation spectroscopy, Journal of Physics: Conference Series 674(1) (2016) 012004.
[20] C.Q. Li, D.K. Xu, B.J. Wang, L.Y. Sheng, Y.X. Qiao, E.H. Han, Natural ageing responses of duplex structured Mg-Li based alloys, Scientific Reports 7(1) (2017) 40078.
[21] I. Stulikova, B. Smola, J. Cizek, T. Kekule, O. Melikhova, H. Kudrnova, Natural and artificial aging in Mg-Gd binary alloys, Journal of Alloys and Compounds 738 (2018) 173-181.
[22] H. Azzeddine, Y.I. Bourezg, A.Y. Khereddine, T. Baudin, A.-L. Helbert, F. Brisset, M. Kawasaki, D. Bradai, T.G. Langdon, An investigation of the stored energy and thermal stability in a Cu–Ni–Si alloy processed by high-pressure torsion, Philosophical Magazine 100(6) (2020) 688-712.
[23] J.-H. Cho, A.D. Rollett, K.H. Oh, Determination of a mean orientation in electron backscatter diffraction measurements, Metallurgical and Materials Transactions A 36(12) (2005) 3427-3438.
[24] R. Hielscher, H. Schaeben, A novel pole figure inversion method: specification of the MTEX algorithm, Journal of Applied Crystallography 41(6) (2008) 1024-1037.
[25] S.K. Das, Y.-B. Kang, T. Ha, I.-H. Jung, Thermodynamic modeling and diffusion kinetic experiments of binary Mg–Gd and Mg–Y systems, Acta Materialia 71 (2014) 164-175.
[26] M. Paliwal, S.K. Das, J. Kim, I.-H. Jung, Diffusion of Nd in hcp Mg and interdiffusion coefficients in Mg–Nd system, Scripta Materialia 108 (2015) 11-14.
[27] N. Stanford, Micro-alloying Mg with Y, Ce, Gd and La for texture modification—A comparative study, Materials Science and Engineering: A 527(10) (2010) 2669-2677.
[28] P. Liu, H. Jiang, Z. Cai, Q. Kang, Y. Zhang, The effect of Y, Ce and Gd on texture, recrystallization and mechanical property of Mg–Zn alloys, Journal of Magnesium and Alloys 4(3) (2016) 188-196.
[29] L. Wang, Y. Li, H. Zhang, Z. Zhang, Q. Yang, Q. Zhang, H. Wang, W. Cheng, K.S. Shin, M. Vedani, Review: Achieving enhanced plasticity of magnesium alloys below recrystallization temperature through various texture control methods, Journal of Materials Research and Technology 9(6) (2020) 12604-12625.
[30] Y.N. Wang, J.C. Huang, Texture analysis in hexagonal materials, Materials Chemistry and Physics 81(1) (2003) 11-26.
[31] B. Kim, J.C. Kim, S. Lee, K.-S. Lee, J.G. Lee, S.S. Park, High-strain-rate superplasticity of fine-grained Mg–6Zn–0.5Zr alloy subjected to low-temperature indirect extrusion, Scripta Materialia 141 (2017) 138-142.

[32] T. Tang, Y. Shao, D. Li, L. Peng, Y. Peng, S. Zhang, P. Wu, Polycrystal plasticity simulation of extrusion of a magnesium alloy round bar: Effect of strain path non-uniformity, Journal of Alloys and Compounds 730 (2018) 161-181.
[33] J. Tang, L. Chen, G. Zhao, C. Zhang, X. Chu, Formation mechanism and evolution of surface coarse grains on a ZK60 Mg profile extruded by a porthole die, Journal of Materials Science & Technology 47 (2020) 88-102.
[34] X. Yang, Y. Okabe, H. Miura, T. Sakai, Annealing of a magnesium alloy AZ31 after interrupted cold deformation, Materials & Design (1980-2015) 36 (2012) 626-632.
[35] F.J. Humphreys, M. Hatherly, Chapter 9 - Recrystallization of Two-Phase Alloys, in: F.J. Humphreys, M. Hatherly (Eds.), Recrystallization and Related Annealing Phenomena (Second Edition), Elsevier, Oxford, 2004, pp. 285-319.
[36] Z.R. Zeng, Y.M. Zhu, S.W. Xu, M.Z. Bian, C.H.J. Davies, N. Birbilis, J.F. Nie, Texture evolution during static recrystallization of cold-rolled magnesium alloys, Acta Materialia 105 (2016) 479-494.
[37] A. Imandoust, C.D. Barrett, T. Al-Samman, M.A. Tschopp, E. Essadiqi, N. Hort, H. El Kadiri, Unraveling Recrystallization Mechanisms Governing Texture Development from Rare-Earth Element Additions to Magnesium, Metallurgical and Materials Transactions A 49(5) (2018) 1809-1829.